Different Ways To Distort a Tetracapped Tetrahedron on Route to Forming an E_4M_4 Cubane: The Case of $[E_4(Pd(PPh_2Me)_2)_4][Ph_2EX_2]_2$ (E = Sb, X = Cl; E = Bi, X = Br)

Joseph L. Stark,[†] Brian Harms,[†] Ilse Guzman-Jimenez,[†] Kenton H. Whitmire,*[,†] Régis Gautier,[‡] Jean-François Halet,[‡] and Jean-Yves Saillard*[,‡]

Contribution from the Department of Chemistry, Rice University, Houston, Texas 77005-1892, and Laboratoire de Chimie du Solide et Inorganique Moléculaire, UMR CNRS 6511, Université de Rennes 1, 35042 Rennes Cedex, France

Received August 12, 1998

Abstract: Tetrakis(diphenylmethylphosphine)palladium reacts with diphenylantimony chloride or diphenylbismuth bromide to give $[E_4(PdL_2)_4][Ph_2EX_2]_2$ (L = PPh_2Me, **1**: E = Sb, X = Cl; **2**: E = Bi, X = Br) which have been characterized spectroscopically and by single-crystal X-ray diffraction for $[Sb_4(PdL_2)_4][Ph_2SbCl_2]_2 \cdot 0.5THF$ and $[Bi_4(PdL_2)_4][Ph_2BiBr_2]_2$. These compounds are electron-rich based on electron counting formalisms. The additional cluster electrons can be rationalized by the ability of group 15 elements to show hypervalency, particularly those elements such as Sb and Bi which show more metal character. The electronic structure of the compounds and of related species has been examined by EHT and DFT calculations. Relationships to other cubane-derived structures are derived, and the stability of structurally related M_4E_4 hypothetical clusters is discussed. Compounds **1** and **2** decompose thermally to give Bi_2Pd and SbPd.

Introduction

The cube, aesthetically satisfying for its high symmetry, is well-represented in elements in both the p-block and d-block and in combinations of the two. The prototypical cubane is C_8H_8, in which the eight carbon atoms occupy the vertices of a regular cube. The most widespread type of cubane structure is that in which two types of vertices are present, A_4B_4, and the different elements occupy alternating vertices:

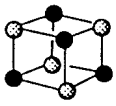

There are now numerous examples in which fragments A and B both are comprised of main group elements. Examples include $[^tBuGa(\mu_3\text{-}E)]_4$ (E = S, Se, Te),[1] $[(R)Ga(\mu_3\text{-}E)]_4$ (R = Me_3C, ^tBu, $EtMe_2C$, Et_2MeC, Et_3C and E = S, Se, Te),[2] $(C_6F_5\text{-}NMMe)_4$ (M = Ga, In),[3] and $(L_nMIn)_4S_4$ (L_nM = $Cp(CO)_2Fe$, $Cp(CO)_3Mo$).[4] Especially numerous are group 13−16 (III−VI) cubane molecules.[4−9] Perhaps the most famous class of cubane structure is that in which **A** is a transition metal fragment (**M**) and **B** is a main group element functionality (**E**). These fragments may be either "naked" or bear a substituent such as an alkyl or aryl group.[10−32] Regular homonuclear cubes of the

[†] Rice University.
[‡] Université de Rennes 1.

(1) (a) Stoll, S. L.; Bott, S. G.; Barron, A. R. *J. Chem. Soc., Dalton Trans.* **1997**, *8*, 1315 and references therein. (b) Power, M. B.; Barron. A. R. *J. Chem. Soc., Chem. Commun.* **1991**, 1315. (c) Power, M. B.; Ziller, J. W.; Barron, A. R. *Organometallics* **1992**, *11*, 1055.
(2) Gillan, E. G.; Bott, S. G.; Barron, A. R. *Chem. Mater.* **1997**, *9*, 806.
(3) Belgardt, T.; Roesky, H. W.; Noltemeyer, M.; Schmidt, H. G. *Angew. Chem., Int. Ed. Engl.* **1993**, *32*, 1056.
(4) Merzweiler, K.; Rudolph, F.; Brands, L. *Naturforsh* **1992**, *47B*, 470.
(5) Uhl, W.; Graupner, R.; Layh, M.; Schütz, U. *J. Organomet. Chem.* **1995**, *493*, C1.
(6) Uhl, W.; Graupner, R.; Pohlmann, M.; Pohl, S.; Saak, W. *Chem. Ber.* **1996**, *129*, 143.
(7) Power, M. B.; Barron, A. R.; Hynk, D.; Robertson, H. E.; Rankin, D. W. H. *Adv. Mater Optics. Electron.* **1995**, *5*, 177.
(8) Harlan, C. J.; Gillan, E. G.; Bott, S. G.; Barron, A. R. *Organometallics* **1996**, *15*, 5479.
(9) Schulz, S.; Andruh, M.; Pape, T.; Heinze, T.; Roesky, H. W.; Haming, L.; Kuhn, A.; Herbst-Irmer, R. *Organometallics* **1994**, *13*, 4004.
(10) Gómez-Sal, P.; Martin, A.; Mena, M.; Yélamon, C. *J. Chem. Soc., Chem. Commun.* **1995**, 2185.
(11) Simon, G. L.; Dahl, L. F. *J. Am. Chem. Soc.* **1973**, *95*, 2175.
(12) Fenske, D.; Basoglu, R.; Hachgenei, J.; Rogel, F. *Angew. Chem., Int. Ed. Engl.* **1984**, *23*, 160.
(13) Scherer, O. J.; Dave, T.; Braun, J.; Wolmershäuser, J. *J. Organomet. Chem.* **1988**, *350*, C20.
(14) Röttinger, E.; Vahrenkamp, H. *Angew. Chem., Int. Ed. Engl.* **1978**, *17*, 273.
(15) Rheingold, A. L.; Foley, M. J.; Sullivan, P. J., *J. Am Chem. Soc.* **1982**, *104*, 4727.
(16) Foust, A. S.; Dahl, L. F. *J. Am. Chem. Soc.* **1970**, *92*, 7337.
(17) Ciani, G.; Moret, M.; Fumagalli, A.; Martinengo, S. *J. Organomet. Chem.* **1989**, *362*, 291.
(18) Röttinger, E.; Vahrenkamp, H. *J. Organomet. Chem.* **1981**, *104*, 4727.
(19) Trinh, T.; Teo, B. K.; Ferguson, J. A.; Meyer, T. J.; Dahl, L. F. *J. Am. Chem. Soc.* **1977**, *99*, 408.
(20) Simon, G. L.; Dahl, L. F. *J. Am. Chem. Soc.* **1973**, *95*, 2164.
(21) Gall, R. S.; Chu, C. T.; Dahl, L. F. *J. Am. Chem. Soc.* **1974**, *96*, 4019.
(22) Gall, R. S.; Connelly, N. G.; Dahl, L. F. *J. Am. Chem. Soc.* **1974**, *96*, 4017.
(23) Wei, C. H.; Wilker, G. R.; Treichel, P. M.; Dahl, L. F. *Inorg. Chem.* **1966,** *5*, 900.
(24) Curtis, M. D.; Williams, P. D. *Inorg. Chem.* **1983**, *22*, 2661.
(25) Schunn, R. A.; Fritchie, C. J., Jr.; Prewitt, C. T. *Inorg. Chem.* **1966**, *5*, 892.
(26) Teo, B. K. *Inorg. Chem.* **1984**, *23*, 1251.
(27) Teo, B. K. *Inorg. Chem.* **1985**, *24*, 4209.
(28) Teo, B. K.; Longoni, G.; Chung, F. R. K. *Inorg. Chem.* **1984**×e2 *24*, 1257.
(29) Harris, S. *Inorg. Chem.* **1987**, *26*, 4278.
(30) Harris, S. *Polyhedron* **1989**, *8*, 2843.
(31) Bahn, C. S.; Tan; A.; Harris, S. *Inorg. Chem.* **1998**, *37*, 2770.
(32) See also: Sung, S.-S.; Glidewell, C.; Butler, A. R.; Hoffmann, R. *Inorg. Chem.* **1985**, *24*, 3856.

10.1021/ja982902u CCC: $18.00
Published on Web 04/27/1999

transition metals are also known, but they have only been found to exist with ligands bridging the square faces or edges and may also possess interstitial atoms.[33−44]

The bonding in a regular cubane is straightforward. Each edge of the cube can be thought to represent a localized 2-center, 2-electron bond. When one considers cubic structures in which metal atoms are present, however, the bonding situations rapidly become more interesting because of the variability in oxidation states which are generally not possible for cubanes made of the lighter main group elements. The metals also possess d-orbitals which allow cross cube bonding interactions. Removal of electrons from the cubane either via redox processes or by change in the electron count of the fragments of A or B may thus be accommodated theoretically by formation of cross cube bonds. The different possible distortions are shown in Scheme 1.

Taking M−M bond formation to its logical completion, one arrives at the tetracapped tetrahedral structure (TT_d) $M_4(\mu_3\text{-}E)_4$. Alternatively, beginning with the TT_d $M_4(\mu_3\text{-}E)_4$ structure, one can derive the cubane structure by successive bond breakage. A number of the structures illustrated have been reported for the class of compounds E_4M_4.[19−25] The compounds have been examined theoretically by Teo and a set of formalisms derived to help explain the pattern of M−M bond formation.[26−28] In the same context, Harris has also provided a qualitative molecular orbital rationalization of the clusters having a M_4S_4 core.[29−32]

What has been missing from the list of known compounds is the alternative bonding pattern $E_4(\mu_3\text{-}M)_4$, in which the core structure is a tetrahedron of main group atoms capped by transition metals. The existence of this inverse bonding scheme was suggested by preliminary calculations.[45] This in an intriguing possibility because the group 15 elements phosphorus and arsenic are known to adopt the E_4 tetrahedron in one allotropic form. Direct reaction of E_4 (E = P, As) has not led to formation of cubane-like derivatives.[46] The predominant outcome has been for the added metal fragments to break E−E bonds and to add to the resulting fragment in $\mu\text{-}E_x$ (x = 2, 4−6) configurations. Cubane structures are known for group 15 and 16 elements arising from other types of reactions which do not begin with an intact E_4 unit. Structurally characterized examples include $[Cp'Ni(\mu_3\text{-}P)]_4$,[13] $E_4\{Fe(CO)_3\}_4$ (E = S, Se, Te),[16] and $E_4\{Co(CO)_3\}_4$ (E = Sb, Bi).[17] These molecules possess no M−M or E−E bonding as anticipated from their electron counts. One molecule that has been identified in which an E_4 core is recognizable and which retains some E−E bonding is the anion $[Bi_4\{Fe(CO)_3\}_3\{Fe(CO)_4\}]^{2-}$ (**12**). In that molecule, three faces of a Bi_4 tetrahedron are capped by $Fe(CO)_3$ groups but the third face remains intact with Bi−Bi distances consistent with single-bond values.[47,48] Two other examples that are structually similar to this are $(Cp^xRu)_3Ru(\eta^3\text{-}As_3)(\mu_3\text{-}\eta^3\text{-}As_3)(\mu_3\text{-}As)_3$ (**13**)[49] and $Cp^*{}_3Fe_3(P_3)(\mu_4\text{-}P)_3Fe(\eta^3\text{-}\mu\text{-}P_3)$ (**14**).[50] Other examples of this rare class of molecule are herein reported.

Scheme 1[a]

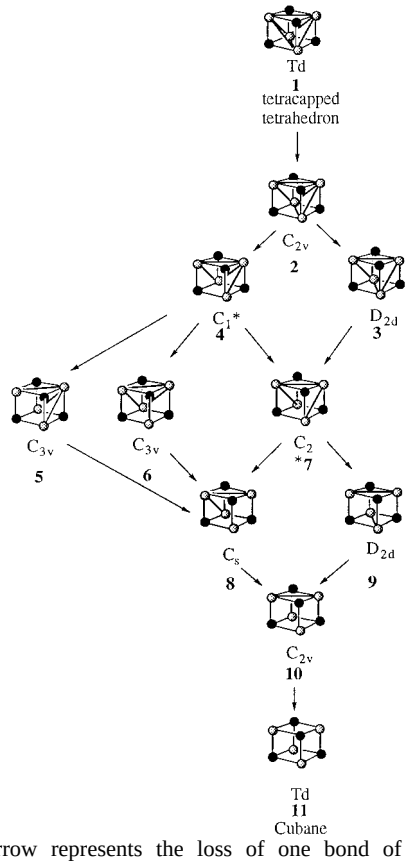

[a] Each arrow represents the loss of one bond of the original tetrahedrom An * denotes a chiral structure.

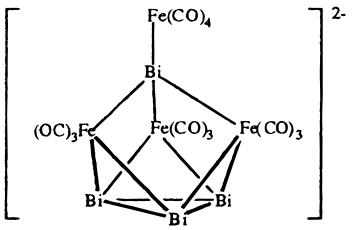

12

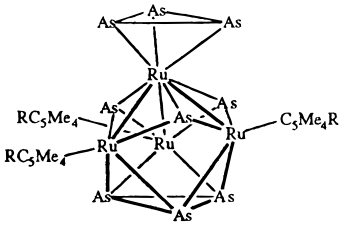

13

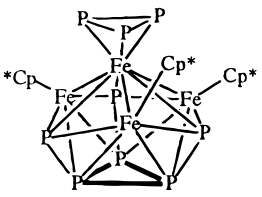

14

(33) Zebrowski, J. P.; Hayashi, R. K.; Bjarnason, A.; Dahl, L. F. *J. Am. Chem. Soc.* **1992**, *114*, 3121.
(34) Fenske, D.; Persau, C. Z. *Anorg. Allg. Chem.* **1991**, *593*, 61.
(35) Fenske, D.; Fleischer, H.; Persau, C. *Angew. Chem., Int. Ed. Engl.* **1989**, *28*, 1665.
(36) Fenske, D.; Ohmer, J.; Merzweiler, K. *Angew. Chem., Int. Ed. Engl.* **1988**, *27*, 1512.
(37) Brennen, J. G.; Siegrist, T.; Stuczyrski, S. M.; Steigerwald, M. L. *J. Am. Chem. Soc.* **1989**, *111*, 9240.
(38) Whitmire, K. H.; Eveland, J. R. *J. Chem. Soc., Chem. Commun.* **1994**, 1335.
(39) Furet, E.; Le Beuze, A.; Halet, J.-F.; Saillard, J.-Y. *J. Am. Chem. Soc.* **1994**, *116*, 274 and references therein.
(40) Furet, E.; Le Beuze, A.; Halet, J.-F.; Saillard, J.-Y. *J. Am. Chem. Soc.* **1995**, *117*, 4936 and references therein.
(41) Halet, J. F.; Saillard, J.-Y. *Struct. Bond.* **1997**, *87*, 81 and references therein.
(42) Rösch, N.; Ackeman, L.; Pacchioni. G. *Inorg. Chem.* **1993**, *32*, 2963.
(43) (a) McCandlish, L. E.; Bissell, E. C.; Coucouvanis, D.; Facker, J. P.; Knox, K. *J. Am. Chem. Soc.* **1968**, *90*, 7357. (b) Hollander, F. J.; Coucouvanis, D. *J. Am. Chem. Soc.* **1974**, *96*, 5646. (c) Avdeef, A.; Fackler, J. P. *Inorg. Chem.* **1978**, *17*, 2182.
(44) (a) Haiduc, I.; Sowerby, D. B.; Lu, S. F. *Polyhedron* **1995**, *14*, 3389. (b) Liu, C. W.; Stubbs, T.; Staples, R. J.; Fackler, J. P. *J. Am. Chem. Soc.* **1995**, *117*, 9778.
(45) Albright, T. A.; Yee, K. A.; Saillard, J.-Y.; Kahlal, K.; Halet, J. F.; Leigh, J. S.; Whitmire, K. H. *Inorg. Chem.* **1991**, *30*, 1179.
(46) Whitmire, K. H. *Adv. Organomet. Chem.* **1998**, *42*, 1.

Experimental Section

Unless otherwise specified, all operations were conducted under an inert atmosphere using standard drybox and Schlenk techniques.[51] All solvents were distilled under nitrogen from appropriate drying agents.[52] ^{1}H and ^{31}P NMR spectra were recorded on a Bruker AC-250 spectrometer, operating at 250 MHz for ^{1}H and 101 MHz for ^{31}P. Infrared spectra were recorded as Nujol mulls on a Perkin-Elmer 1640 spectrophotometer. The compounds Ph_2SbCl[53] and Ph_2BiBr[54] were prepared by literature methods. The compound $Pd[PPh_2Me]_4$ was purchased from Aldrich and used as received. Powder X-ray diffraction patterns were recorded on a Siemens 5000 powder diffractometer. Elemental analyses were performed by Desert Analytics.

Preparation of $[Sb_4\{Pd(PPh_2Me)_2\}_4][Ph_2SbCl_2]_2$ (1). Solid portions of PdL_4 (0.15 g, 0.16 mmol) and Ph_2SbCl (0.051 g, 0.16 mmol) were weighed into a flask, dissolved in tetrahydrofuran (30 mL), and stirred at room temperature for 15 h, during which time the solution became dark red to black and a precipitate developed. The volume of solution was reduced to ca. 5 mL. The dark red solid was collected by filtration, washed twice with ether (ca. 30 mL), and then dried under vacuum. Crystals suitable for X-ray diffraction were obtained by dissolving PdL_4 (0.029 g, 0.032 mmol) into 2 mL of THF in a 12 × 75 mm test tube and then suspending Ph_2SbCl (0.01 g, 0.032 mmol) on top of the solution. Block-shaped crystals deposited over a period of 1 week at room temperature. Yields were typically 15% yield. Anal. Calcd for $C_{130}H_{128}O_{0.5}Cl_4P_8Pd_4Sb_6$ (**1**·0.50C_4H_8O): C, 48.15; H, 3.98; P, 7.64. Found: C, 49.35; H, 3.99; P, 8.12. ^{1}H NMR (CD_2Cl_2) 27 °C: δ 7.72 (m, *o*-H, Ph), 7.17 (m, *m*,*p*-H, Ph), 1.98 (d, J_{P-H} = 1.4 Hz, 24 H, Me) ^{31}P NMR (CD_2Cl_2): δ −9.06 (s, PPh_2Me). NMR analyses of the reaction solution showed free phosphine and L_2PdCl_2 as byproducts of the reaction, but these were not quantitated.

Preparation of $[Bi_4\{Pd(PPh_2Me)_2\}_4][Ph_2BiBr_2]_2$ (2). Solid PdL_4 (0.15 g, 0.16 mmol) was added to a solution of Ph_2BiBr (0.073 g, 0.16 mmol) in THF (30 mL) and stirred for 15 h, forming a black solution that contained a precipitate. The volume of the solution was reduced to ca. 5 mL, after which the solid was collected by filtration, washed twice with ether (ca 30 mL), and dried under vacuum. Crystals suitable for X-ray diffraction were obtained by dissolving PdL_4 (0.0205 g, 0.023 mmol) and Ph_2BiBr (0.01 g, 0.023 mmol) into 2 mL of THF in a 12 × 75 mm test tube and allowing the test tube to stand for 1 week. Yields were typically 16% yield. Anal. Calcd for $C_{128}H_{124}Br_4P_8Pd_4Bi_6$: C, 39.33; H, 3.20; P, 6.34. Found: C, 39.23; H, 3.60; P, 6.70. ^{1}H NMR (CD_2Cl_2, 27° C): δ 7.72 (m, *o*-H, Ph), 7.17 (m, *m*,*p*-H, Ph), 1.95 (d, J_{P-H} = 1.4 Hz, 24 H, Me). ^{31}P NMR (CD_2Cl_2): δ −4.23 (s, PPh_2Me). NMR analyses of the reaction solution showed free phosphine and L_2PdBr_2 as byproducts of the reaction, but these were not quantitated.

Formation of PdSb (3). A portion of **1** (44 mg, 0.014 mmol) was initially suspended in 50 mL of toluene and refluxed overnight. The toluene was filtered off, and the residual black solid was placed in a platinum pan and heated to 600 °C for 1 h under argon, after which time the sample was cooled to give 10 mg of black polycrystalline material, which was an 80% yield based upon Pd. Formation of polycrystalline PdSb was confirmed by powder X-ray crystallography.

Formation of Bi_2Pd (4). Compound **2** (60 mg, 0.015 mmol) was suspended into 50 mL of toluene and refluxed overnight to give a black precipitate. The toluene was filtered off, and the black residue was placed in a platinum pan and heated for 1 h at 600 °C under argon to give black polycrystalline material. Formation of Bi_2Pd was confirmed by powder X-ray diffraction analysis. Yield: 8 mg (0.15 mmol) of black polycrystalline material was recovered, making the yield 33% (based on Bi) for formation of Bi_2Pd.

Table 1. Crystallographic Data for $[Sb_4\{Pd(Ph_2PMe)_2)_4]$-$[Ph_2SbCl_2]_2$·0.5THF (**1**) and $[Bi_4\{Pd(Ph_2PMe)_2)_4][Ph_2BiBr_2]_2$ (**2**)[a]

empirical formula	$C_{130}H_{128}Cl_4O_{0.50}P_8Pd_4Sb_6$	$C_{128}H_{124}Bi_6Br_4P_8Pd_4$
formula weight	3243.98	3909.15
crystal system	triclinic	triclinic
space group	$P\bar{1}$	$P\bar{1}$
a (Å)	14.176(3)	14.395(3)
b (Å)	14.770(3)	14.974(3)
c (Å)	32.465(7)	32.363(7)
α (deg)	85.08(3)	84.75(3)
β (deg)	77.96(3)	77.78(3)
γ (deg)	85.23(3)	85.59(3)
V (Å^3)	6608.6(23)	6777.3(24)
Z	2	2
GOF on F^2	1.108	1.039
final *R* indices [$I > 2\sigma(I)$]	$R1 = 0.0386$	$R1 = 0.0550$
R indices (all data)	w$R2 = 0.1334$	w$R2 = 0.1658$

[a] $w = I/[\sigma^2(F_o^2) + (0.0867P)^2]$, $w = I/[(\sigma^2(F_o^2) + (0.0200P)^2 + 35.9373P]$, $P = (F_o^2 + 2F_c^2)/3$.

Single-Crystal X-ray Diffraction Studies of 1 and 2. Data were collected on a Rigaku AFC5S fully automated, four-circle single-crystal X-ray diffractometer (Rigaku CONTROL Automatic Data Collection Series, Molecular Structure Corp., The Woodlands, TX)[55] using graphite monochromated Mo Kα radiation (0.7107 Å). Data collection and refinement parameters are given in Table 1. The crystals were mounted on a glass fiber with Epoxy cement, and data were collected with ω scans at 4 deg/min. Three standard reflections were monitored for decay every 150 reflections throughout data collection. An absorption correction from azimuthal (ψ) scans was applied to each data set. The programs used in solving each structure were part of the Siemens Analytical X-ray Instruments data reduction and refinement package SHELXTL PC,[56] and refinement of each structure was performed using the data refinement program package SHELXL-93.[57] The scattering factors used were those found in the *International Tables for X-ray Crystallography*.[58]

Computational Details. (a) Extended Hückel Calculations. Calculations have been carried out within the extended Hückel formalism[59] using the weighted H_{ij} formula[60] with the program CACAO.[61] The exponents (ζ) and the valence shell ionization potentials (H_{ii} in eV) were (respectively): 1.3, −13.6 for H 1s; 1.625, −24.4 for C 2s; 1.625, −11.4 for C 2p; 2.275, −32.3 for O 2s; 2.275, −14.8 for O 2p; 1.6, −18.6 for P 3s; 1.6, −14.0 for P 3p; 2.323, −18.8 for Sb 5s; 1.999, −11.7 for Sb 5p; 1.9, −9.10 for Fe 4s; 1.9, −5.32 for Fe 4p; 2.19, −7.32 for Pd 5s; 2.152, −3.75 for Pd 5p. H_{ii} values for Fe 3d and Pd 4d were set equal to −12.6 and −12.02, respectively. A linear combination of two Slater-type orbitals of exponents $\zeta_1 = 5.35$, $\zeta_2 = 1.80$ and $\zeta_1 = 5.983$, $\zeta_2 = 2.613$ with the weighting coefficients $c_1 = 0.5366$, $c_2 = 0.6678$ and $c_1 = 0.5264$, $c_2 = 0.6373$ were used to represent the Fe 3d and Pd 4d atomic orbitals, respectively. The following bond distances (Å) and angles (deg) were used in the T_d $Fe_4(CO)_{12}(\mu_3\text{-Sb})_4$ model: Fe−Sb = 2.50, Sb−Sb = 3.05, Fe−C = 1.85, C−O = 1.15. The molecular model $Sb_4[\mu_3\text{-Pd}(PH_3)_2]_4$ used was based on the averaged idealized (D_{2d}) experimental structure of **1**. The

(47) Whitmire, K. H.; Albright, T. A.; Kang, A.-K.; Churchill, M. R. Fettinger, J. C. *Inorg. Chem.* **1986**, *25*, 2799.
(48) Whitmire, K. H.; Churchill, M. R.; Fettinger, J. C. *J. Am. Chem. Soc*. **1985**, *107*, 1056.
(49) Scherer, O. J.; Blath, C.; Heckmann, G.; Wolmershäuser. *J. Organomet. Chem*. **1991**, *409*, C15.
(50) Ahlrichs, R.; Fenske, D.; Fromm, K. Krautscheid, H.; Treutler, O. *Chem. Eur. J.* **1996**, *2*, 238.
(51) Shriver, D. F.; Drezdon, M. A. *The Manipulation of Air-Sensitive Compounds*; Wiley: New York, 1986.
(52) (a) Gordon, A. J.; Ford, R. A. *The Chemist's Companion*; John Wiley and Sons: New York, 1972. (b) Pangborn, A. B.; Giardello, M. A.; Grubbs, R. H.; Rosen, R. K.; Timmers, F. J. *Organometallics* **1996**, *15*, 1518.
(53) Nunn, M.; Sowerby, D. B.; Wesolek, D. M. *J. Organomet. Chem.* **1983**, *251*, C45.
(54) Wilkinson, J. F.; Challenger, F. *J. Chem. Soc.* **1924**, 12.
(55) *TEXSAN: Single-Crystal Structure Analysis Software 5.0*, Molecular Structure Co., The Woodlands, TX, 1990.
(56) Sheldrick, G. M. *SHELXTL PLUS PC 5.0*, Siemens Crystallographic Research Systems, Madison, WI, 1995.
(57) Shedrick, G. M. *SHELXL-93*, Göttingen, Germany, 1993.
(58) *International Tables for Crystallography*; Kluwer Academic Publishers: Dordrecht, The Netherlands, 1992; Vol. C; Tables 4.2.6.8. and 6.1.1.4.
(59) Hoffmann, R. *J. Chem. Phys.* **1963**, *39*, 1397.
(60) Ammeter, J. H.; Bürgi, H.-B.; Thibeault, J. C.; Hoffmann, R. *J. Am. Chem. Soc.* **1978**, *100*, 3686.
(61) Mealli, C.; Proserpio, D. *J. Chem. Educ.* **1990**, *67*, 399.

following bond distances (Å) were used in this model: Pd−Sb = 2.64 and 2.76, Sb−Sb = 3.05 and 3.39, Pd−P = 2.36, P−H = 1.42.

(b) Density Functional Calculations. Density functional calculations[62] were carried out on $[Sb_4Fe_4(CO)_{12}]^{2+}$, $[Sb_4Pd_4(PH_3)_8]^{2+}$, $E_4Co_4(CO)_{12}$ (E = Bi, Sb), and $[E'_4\{\mu_3\text{-}Fe(CO)_3\}_4]^{2+}$ (E = Ga, In, Tl), using the Amsterdam Density Functional (ADF) program.[63] Electron correlation was treated within the local density approximation (LDA).[64] The numerical integration procedure applied for the calculations was developed by te Velde et al.[65] The atom electronic configurations were described by a triple-ζ Slater-type orbital (STO) basis set for H 1s, C 2s and 2p, O 2s and 2p, P 3s and 3p, Ga 3d, 4s, and 4p, In 4d, 5s, and 5p, Sb 4d, 5s, and 5p, Tl 5d, 6s, and 6p, Bi 5d, 6s, and 6p, Fe 4s and 3d, Co 4s and 3d, Pd 5s and 4d and single-ζ STO function for H 2p, C 3d, O 3d, P 3d, Ga 4d, Fe 4p, Co 4p and Pd 5p. The frozen-core approximation[66] was used.

Results

Formation of **1** and **2** occurs by the direct addition of 1 equiv of PdL_4 to 1 equiv of either Ph_2SbCl or Ph_2BiBr (eq 1).

$$PdL_4 + Ph_2EX \rightarrow [E_4\{PdL_2\}_4][Ph_2EX_2] + ... \quad (1)$$

1: E = Sb, X = Cl; **2**: E = Bi, X = Br; L = PPh_2Me

The reactions were performed in dry THF and led to the formation of dark red crystals for **1** in 15% yield and black blocklike crystals for **2** in 16% yield. The compounds are not soluble in most organic solvents. They are sparingly soluble in acetonitrile and in methylene chloride; however, dissolving the compounds in any solvent leads to slow decomposition of the products which contributes to the low isolated yields. The decomposition was evident while attempting to obtain ^{31}P NMR of the products. Upon dissolving **1** or **2** in CD_2Cl_2 and immediately collecting the NMR data, one resonance was observed for **1** at $\delta = -9.06$ ppm and for **2** at $\delta = -4.23$ ppm. If the samples are allowed to set for any period of time other resonances begin to appear for **1** at $\delta = 28.2$ and 8.8 ppm and for **2** at $\delta = 28.2$ and 7.4 ppm. The signal at $\delta = 28.2$ ppm is due to the presence of free PPh_2Me, but determination of the nature of the other compound(s) has not yet been successful. If excess Ph_2EX is used, L_2PdX_2 is formed.

Taking the lability of the phosphine ligands into consideration, an attempt was made to utilize the clusters as molecular precursors for the synthesis of solid-state compounds. Following the work of Steigerwald and co-workers on metal tellurides,[67] **1** and **2** were pyrolyzed in refluxing toluene to generate antimony−palladium and bismuth−palladium solid-state compounds. Upon pyrolysis, black precipitates were obtained but the materials produced in this fashion are amorphous. Subsequent thermolysis of the black precipitates at 600 °C for 1 h under argon led to the formation of black polycrystalline material. Powder X-ray diffraction measurements confirmed the compounds to be polycrystalline SbPd (**3**) from **1** and Bi_2Pd (**4**) from **2**. These pyrolyses led to the thermodynamically stable phases and, given the differing compositions of the Sb and Bi alloys, must be independent of the starting cluster E−M stoichiometry.

(62) (a) Baerends, E. J.; Ellis, D. E.; Ros, P. *Chem. Phys.* **1973**, *2*, 41. (b) Baerends, E. J.; Ros, P. *Int. J. Quantum. Chem.* **1978**, *S12*, 169. (c) te Velde, G.; Baerends, E. J. *J. Comput. Phys.* **1992**, *99*, 84.

(63) Baerends E. J.; et al. *Amsterdam Density Functional (ADF) program*, version 2.3, Vrije Universiteit, Amsterdam, Netherlands, 1997.

(64) Vosko, S. D.; Wilk, L.; Nusair, M. *Can. J. Chem.* **1980**, *58*, 1200.

(65) Boerrigter, P. M.; te Velde, G.; Baerends, E. J. *Int. J. Quantum Chem.* **1988**, *33*, 87.

(66) Baerends, E. J. Ph.D. Thesis, Vrije Universiteit, Amsterdam, Netherlands, 1975.

(67) Steigerwald, M. L.; Rice, C. E. *J. Am. Chem. Soc.* **1988**, *110*, 4228.

Table 2. Selected Bond Lengths (Å) and Angles (deg) for $[Sb_4\{Pd(PPh_2Me)_2\}_4][Ph_2ECl_2]_2\cdot 0.5THF$ (**1**)

Bond Lengths			
Sb(1)−Pd(2)	2.6380(10)	Sb(1)−Pd(3)	2.6662(10)
Sb(1)−Pd(1)	2.8245(10)	Sb(1)−Sb(3)	3.0442(12)
Sb(1)−Sb(2)	3.0726(10)	Sb(2)−Pd(4)	2.6288(11)
Sb(2)−Pd(1)	2.6501(10)	Sb(2)−Pd(2)	2.7734(10)
Sb(2)−Sb(4)	3.0530(12)	Sb(3)−Pd(1)	2.6358(10)
Sb(3)−Pd(4)	2.6508(9)	Sb(3)−Pd(3)	2.7745(10)
Sb(3)−Sb(4)	3.0920(13)	Sb(4)−Pd(3)	2.6273(9)
Sb(4)−Pd(2)	2.6705(12)	Sb(4)−Pd(4)	2.8059(9)
Pd(1)−P(2)	2.355(2)	Pd(1)−P(1)	2.375(2)
Pd(2)−P(3)	2.369(2)	Pd(2)−P(4)	2.374(2)
Pd(3)−P(6)	2.362(2)	Pd(3)−P(5)	2.376(2)
Pd(4)−P(7)	2.359(2)	Pd(4)−P(8)	2.361(2)
Bond Angles			
Pd(2)−Sb(1)−Pd(3)	89.18(4)	Pd(2)−Sb(1)−Pd(1)	110.44(4)
Pd(3)−Sb(1)−Pd(1)	110.82(4)	Pd(2)−Sb(1)−Sb(3)	105.24(4)
Pd(3)−Sb(1)−Sb(3)	57.68(3)	Pd(1)−Sb(1)−Sb(3)	53.22(2)
Pd(2)−Sb(1)−Sb(2)	57.51(2)	Pd(3)−Sb(1)−Sb(2)	103.27(3)
Pd(1)−Sb(1)−Sb(2)	53.21(3)	Sb(3)−Sb(1)−Sb(2)	67.72(3)
Pd(4)−Sb(2)−Pd(1)	86.42(4)	Pd(4)−Sb(2)−Pd(2)	112.82(4)
Pd(1)−Sb(2)−Pd(2)	111.67(4)	Pd(4)−Sb(2)−Sb(4)	58.62(2)
Pd(1)−Sb(2)−Sb(4)	103.82(4)	Pd(2)−Sb(2)−Sb(4)	54.30(3)
Pd(4)−Sb(2)−Sb(1)	102.90(3)	Pd(1)−Sb(2)−Sb(1)	58.60(2)
Pd(2)−Sb(2)−Sb(1)	53.35(3)	Sb(4)−Sb(2)−Sb(1)	66.62(3)
Pd(1)−Sb(3)−Pd(4)	86.27(3)	Pd(1)−Sb(3)−Pd(3)	113.34(4)
Pd(4)−Sb(3)−Pd(3)	110.50(4)	Pd(1)−Sb(3)−Sb(1)	59.12(3)
Pd(4)−Sb(3)−Sb(1)	103.12(3)	Pd(3)−Sb(3)−Sb(1)	54.30(3)
Pd(1)−Sb(3)−Sb(4)	103.12(4)	Pd(4)−Sb(3)−Sb(4)	57.89(2)
Pd(3)−Sb(3)−Sb(4)	52.88(3)	Sb(1)−Sb(3)−Sb(4)	66.48(3)
Pd(3)−Sb(4)−Pd(2)	89.31(3)	Pd(3)−Sb(4)−Pd(4)	110.23(4)
Pd(2)−Sb(4)−Pd(4)	110.52(4)	Pd(3)−Sb(4)−Sb(2)	104.76(3)
Pd(2)−Sb(4)−Sb(2)	57.50(2)	Pd(4)−Sb(4)−Sb(2)	53.12(3)
Pd(3)−Sb(4)−Sb(3)	57.35(2)	Pd(2)−Sb(4)−Sb(3)	103.15(3)
Pd(4)−Sb(4)−Sb(3)	53.15(3)	Sb(2)−Sb(4)−Sb(3)	67.37(3)
Sb(3)−Pd(1)−Sb(2)	80.30(4)	Sb(3)−Pd(1)−Sb(1)	67.67(4)
Sb(2)−Pd(1)−Sb(1)	68.20(3)	Sb(1)−Pd(2)−Sb(4)	78.64(4)
Sb(1)−Pd(2)−Sb(2)	69.14(3)	Sb(4)−Pd(2)−Sb(2)	68.19(3)
Sb(4)−Pd(3)−Sb(1)	78.90(3)	Sb(4)−Pd(3)−Sb(3)	69.77(3)
Sb(1)−Pd(3)−Sb(3)	68.01(4)	Sb(2)−Pd(4)−Sb(3)	80.41(3)
Sb(2)−Pd(4)−Sb(4)	68.26(3)	Sb(3)−Pd(4)−Sb(4)	68.96(3)

Structures of 1·0.5THF and 2. The crystal data for **1**·0.5THF and **2** (Table 1) show the two structures to be isomorphous, consisting of 2:1 ratios of $[Ph_2EX_2]^-$ ions to $[E_4\{PdL_2\}_4]^{2+}$ dications (E = Sb, X = Cl; E = Bi, X = Br). One of the anions for **1**·0.5THF and for **2** has disordered aromatic rings. For **1**·0.5THF, both of the rings of that one anion showed resolvable disorder components, but for **2**, disorder for only one of the rings could be resolved. The second ring has slightly larger than normal thermal ellipsoids, suggesting that it also has disorder, but it was not resolvable. Thermal ellipsoid plots of these anions showing the disorder components are included in the Supporting Information. Selected bond distances and angles are found in Tables 2 and 3 for **1**·0.5THF and **2**. Thermal ellipsoid plots of the metal cores of the cations are provided in Figures 1 and 2. For **1**·0.5THF there is also one-half of a THF molecule per cluster unit in the crystalline lattice (located on a general position but only at half-occupancy). Despite the fact that the two compounds are isomorphous, no lattice solvent was found in the structure for **2** and the elemental analyses are consistent with a solventless formulation.

The four main group atoms define a pseudo-tetrahedron in which the triangular faces are capped by μ_3-PdL_2 fragments. The Pd atoms are ligated by three E atoms and two phosphine ligands in a distorted square pyramidal array. The longest Pd−E distances are those to the E atoms in the apical positions. For **1**·0.5THF the range is $Pd-Sb_{apical}$ = 2.7734(10)−2.8245(10) Å vs $Pd-Sb_{basal}$ = 2.6273(9)−2.6705(12) Å), while for **2** Pd−

Table 3. Selected Bond Lengths (Å) and Angles (deg) for $[Bi_4\{Pd(Ph_2PMe)_2\}_4][Ph_2BiBr_2]_2$ (**2**)

Bond Lengths			
Bi(1)−Pd(2)	2.730(2)	Bi(1)−Pd(3)	2.763(2)
Bi(1)−Pd(1)	2.957(2)	Bi(1)−Bi(3)	3.201(2)
Bi(1)−Bi(2)	3.2194(13)	Bi(1)−Bi(4)	3.4518(13)
Bi(2)−Pd(4)	2.715(2)	Bi(2)−Pd(1)	2.745(2)
Bi(2)−Pd(2)	2.887(2)	Bi(2)−Bi(4)	3.2177(14)
Bi(2)−Bi(3)	3.5093(14)	Bi(3)−Pd(1)	2.718(2)
Bi(3)−Pd(4)	2.748(2)	Bi(3)−Pd(3)	2.892(2)
Bi(3)−Bi(4)	3.239(2)	Bi(4)−Pd(3)	2.716(2)
Bi(4)−Pd(2)	2.765(2)	Bi(4)−Pd(4)	2.912(2)
Pd(1)−P(2)	2.343(5)	Pd(1)−P(1)	2.352(5)
Pd(2)−P(4)	2.346(6)	Pd(2)−P(3)	2.355(6)
Pd(3)−P(6)	2.350(6)	Pd(3)−P(5)	2.353(5)
Pd(4)−P(7)	2.344(5)	Pd(4)−P(8)	2.347(5)

Bond Angles			
Pd(2)−Bi(1)−Pd(3)	91.93(6)	Pd(2)−Bi(1)−Pd(1)	109.56(6)
Pd(3)−Bi(1)−Pd(1)	109.46(6)	Pd(2)−Bi(1)−Bi(3)	105.09(5)
Pd(3)−Bi(1)−Bi(3)	57.46(4)	Pd(1)−Bi(1)−Bi(3)	52.21(4)
Pd(2)−Bi(1)−Bi(2)	57.36(4)	Pd(3)−Bi(1)−Bi(2)	103.54(5)
Pd(1)−Bi(1)−Bi(2)	52.57(4)	Bi(3)−Bi(1)−Bi(2)	66.27(3)
Pd(2)−Bi(1)−Bi(4)	51.53(4)	Pd(3)−Bi(1)−Bi(4)	50.35(4)
Pd(1)−Bi(1)−Bi(4)	93.75(5)	Bi(3)−Bi(1)−Bi(4)	58.13(3)
Bi(2)−Bi(1)−Bi(4)	57.55(3)	Pd(4)−Bi(2)−Pd(1)	88.88(5)
Pd(4)−Bi(2)−Pd(2)	111.29(6)	Pd(1)−Bi(2)−Pd(2)	111.18(5)
Pd(4)−Bi(2)−Bi(4)	58.05(4)	Pd(1)−Bi(2)−Bi(4)	103.43(5)
Pd(2)−Bi(2)−Bi(4)	53.52(4)	Pd(4)−Bi(2)−Bi(1)	102.84(4)
Pd(1)−Bi(2)−Bi(1)	58.80(4)	Pd(2)−Bi(2)−Bi(1)	52.77(4)
Bi(4)−Bi(2)−Bi(1)	64.86(3)	Pd(4)−Bi(2)−Bi(3)	50.44(4)
Pd(1)−Bi(2)−Bi(3)	49.70(4)	Pd(2)−Bi(2)−Bi(3)	94.51(5)
Bi(4)−Bi(2)−Bi(3)	57.37(3)	Bi(1)−Bi(2)−Bi(3)	56.61(3)
Pd(1)−Bi(3)−Pd(4)	88.77(5)	Pd(1)−Bi(3)−Pd(3)	112.71(6)
Pd(4)−Bi(3)−Pd(3)	109.32(5)	Pd(1)−Bi(3)−Bi(1)	59.28(4)
Pd(4)−Bi(3)−Bi(1)	102.57(4)	Pd(3)−Bi(3)−Bi(1)	53.64(4)
Pd(1)−Bi(3)−Bi(4)	103.50(5)	Pd(4)−Bi(3)−Bi(4)	57.50(4)
Pd(3)−Bi(3)−Bi(4)	52.22(4)	Bi(1)−Bi(3)−Bi(4)	64.82(3)
Pd(1)−Bi(3)−Bi(2)	50.38(4)	Pd(4)−Bi(3)−Bi(2)	49.62(4)
Pd(3)−Bi(3)−Bi(2)	94.19(5)	Bi(1)−Bi(3)−Bi(2)	57.12(3)
Bi(4)−Bi(3)−Bi(2)	56.78(3)	Pd(3)−Bi(4)−Pd(2)	92.19(6)
Pd(3)−Bi(4)−Pd(4)	109.63(5)	Pd(2)−Bi(4)−Pd(4)	109.14(6)
Pd(3)−Bi(4)−Bi(2)	104.68(5)	Pd(2)−Bi(4)−Bi(2)	57.12(4)
Pd(4)−Bi(4)−Bi(2)	52.29(4)	Pd(3)−Bi(4)−Bi(3)	57.30(4)
Pd(2)−Bi(4)−Bi(3)	103.26(5)	Pd(4)−Bi(4)−Bi(3)	52.74(4)
Bi(2)−Bi(4)−Bi(3)	65.84(3)	Pd(3)−Bi(4)−Bi(1)	51.55(4)
Pd(2)−Bi(4)−Bi(1)	50.64(4)	Pd(4)−Bi(4)−Bi(1)	93.50(5)
Bi(2)−Bi(4)−Bi(1)	57.60(3)	Bi(3)−Bi(4)−Bi(1)	57.05(3)
Bi(3)−Pd(1)−Bi(2)	79.93(5)	Bi(3)−Pd(1)−Bi(1)	68.51(5)
Bi(2)−Pd(1)−Bi(1)	68.63(5)	Bi(1)−Pd(2)−Bi(4)	77.83(5)
Bi(1)−Pd(2)−Bi(2)	69.87(5)	Bi(4)−Pd(2)−Bi(2)	69.36(5)
Bi(4)−Pd(3)−Bi(1)	78.10(5)	Bi(4)−Pd(3)−Bi(3)	70.48(5)
Bi(1)−Pd(3)−Bi(3)	68.90(5)	Bi(2)−Pd(4)−Bi(3)	79.94(5)
Bi(2)−Pd(4)−Bi(4)	69.66(5)	Bi(3)−Pd(4)−Bi(4)	69.76(5)

Bi_{apical} = 2.887(2)−2.957(2) Å vs Pd−Bi_{basal} = 2.715(2)−2.765(2) Å). If one neglects the apical E atoms, the Pd atoms can be considered to have the common *cis*-L_2PdX_2 geometry, but the calculations indicate that the bonding to the apical E atom is significant (vide infra). Only four E−E distances of the six present in the tetrahedral array may be considered bonding, even though they are somewhat long. For **1**·0.5THF these four bonding distances are 3.0442(12)−3.0920(12) Å versus two nonbonding distances of 3.36−3.41 Å. They may be compared to the Sb−Sb interactions in the pure crystalline element (2.908 and 3.355 Å).[68] Similarly, the Bi−Bi bonding distances observed for **2** (3.201(2)−3.239(2) Å) and nonbonding interactions (3.45−3.51 Å) may be compared to the Bi−Bi contacts observed in the pure crystalline element (3.07 and 3.53 Å).[69] The presence of only four E−E bonding interactions, whose nature will be more extensively examined in the theoretical discussion, gives the $[E_4(PdL_2)_4]^{2+}$ clusters idealized D_{2d} symmetry.

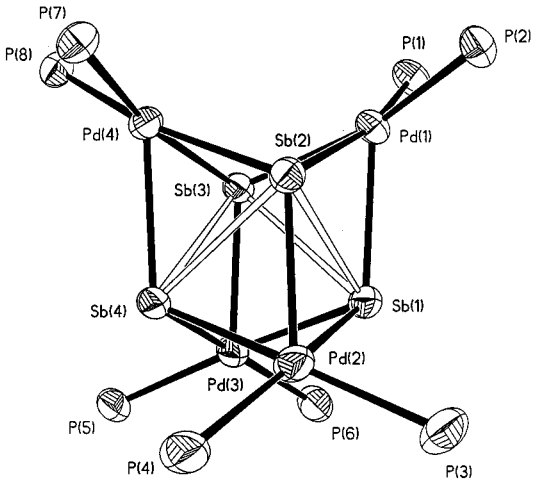

Figure 1. Thermal ellipsoid plot (50% probability level) of the cationic portion of the cluster $[Sb_4(PdL_2)_4][Ph_2SbCl_2]_2$·0.5THF. The carbon atoms have been omitted for clarity. Full thermal ellipsoid plots and labeling scheme are provided in the Supporting Information.

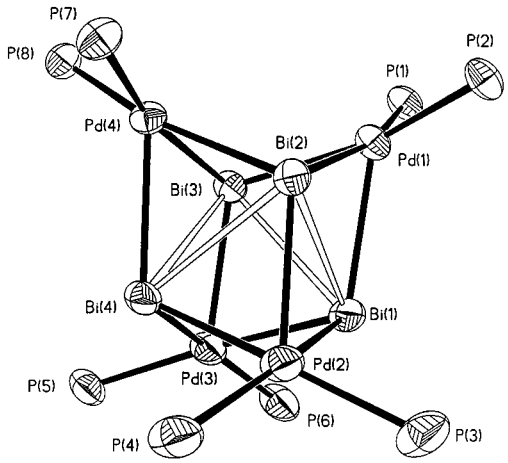

Figure 2. Thermal ellipsoid plot (50% probability level) of the cationic portion of the cluster $[Bi_4(PdL_2)_4][Ph_2BiBr_2]_2$. The carbon atoms have been omitted for clarity. Full thermal ellipsoid plots and labeling scheme are available in the Supporting Information.

The Pd−Sb distances in **1**·0.5THF may also be compared to those observed in $[Sb_6Pd_9(PPh_3)_8]$, which is essentially a Pd_8 cube with a Pd atom residing in the center of the cube and μ_5-Sb atoms capping each face of the cube. Here there is also one long Pd−Sb distance, that of the center Pd to the bridging Sb atoms (2.868(1) Å), and two short Pd−Sb distances (2.621(1) and 2.601(1) Å). The alloy PdSb, which is formed by pyrolysis of compound **1**, shows a Pd−Sb distance (2.737 Å) intermediate to the bonding and nonbonding distances of compound **1**.[70]

Compound **2** may be compared to the $[Bi_4Fe_4(CO)_{13}]^{2-}$ dianion.[71] In this molecule the four bismuth atoms define a tetrahedron in which three triangular faces are capped by μ_3-$Fe(CO)_3$ fragments and a fourth face is bare. There are two unique Bi−Bi distances (ca. 3.16 and 3.46 Å) that compare favorably to those observed in **2**. The Bi_4^{2-} anion has been crystallographically characterized and can be viewed as a square-planar array of Bi atoms with two unique Bi−Bi distances of

(68) Barrett, C. S.; Cucka, P.; Haefner, K. *Acta Crystallogr.* **1963**, *16*, 451.

(69) Cucka, P.; Barrett, C. S. *Acta Crystallogr.* **1962**, *15*, 865.

(70) Pratt, J. N.; Myles, K. M.; Darby, J. B., Jr.; Mueller, M. H. *J. Less Common Met.* **1968**, *14*, 427.

(71) Whitmire, K. H.; Albright, T. A.; Kang, S.-K.; Churchill, M. R.; Fettinger, J. C. *Inorg. Chem.* **1986**, *25*, 2799.

2.936(2) and 2.941(2) Å.[72] Those distances are considerably shorter and are thought to arise due to multiple-bonding interactions in the square-planar molecule which is an aromatic, 6π-electron system. The tetragonal phase of the β-Bi_2Pd alloy has a known crystal stucture, and was the phase isolated from the thermolysis of cluster **2**. This Bi_2Pd alloy has sheets of cubic arrays of Bi atoms with the cubes centered by Pd atoms.[73] The Bi−Pd distances of the alloy (2.969 Å) are slightly longer than the long Bi−Pd distances of **2**. The two Bi−Bi distances (3.362 and 3.557 Å) observed in the alloy are comparable to the nonbonding Bi−Bi contacts in **2**.

Discussion

A number of synthetic methodologies reviewed elsewhere have been developed for preparing E−M cluster compounds.[46] Our interest in compounds with Pd arose from the possibility of using the well-established ability of the noble metals to undergo oxidative-addition reactions into E−X bonds. We anticipated that the first step of a reaction between organo main group halides where the main group element was a heavy atom such as Bi or Sb and a Pd^0 complex would be insertion of the Pd into the E−X bond as illustrated in eq 2.

$$Ph_2EX + PdL_4 \rightarrow L_2Pd(EPh_2)(X) + 2L \qquad (2)$$

$$Ph_2EX + X^- \rightarrow [Ph_2EX_2]^- \qquad (3)$$

We have observed empirically that organic groups attached to metalated heavy main group elements are extremely easily lost and intended to use such compounds as intermediates in the formation of cluster compounds. In this case, however, this hypothesis evidently works so well that an intermediate $PdEPh_2$ complex is not observed and a cluster compound is the product isolated directly from the reaction. These compounds have the formulation $[E_4(PdL_2)_4][Ph_2EX_2]_2$ (E = Sb, X = Cl; E = Bi, X = Br) and are obtained directly from the reaction of PdL_4 and the appropriate Ph_2EX. One of the most interesting features of the product is the cationic nature of the cluster core. Most cluster compounds are either negatively charged or neutral with positively charged species being extremely rare. In many cases, those that are known possess hydride ligands and could be consider as protonated compounds, which is not the case here.

The reaction mechanism is obviously complex, but it is clear from the product formulation that Ph_2EX has been used to scavenge halide ions, a well-precedented process for organobismuth and antimony halide compounds (eq 3) in their direct reaction with free X^-.[75,75] The dibromodiphenylbismuthide and dichlorodiphenylantimonide ions are readily formed by adding the appropriate tetraphenylphosphonium halide to either Ph_2BiBr(thf) or in the case of antimony to either $PhSbX_2$ or Ph_2SbX. It is possible that Ph_2EX may abstract a halide ion directly from an intermediate $L_2Pd(EPh_2)(X)$ to give $L_2Pd(EPh_2)^+$.

There is a significant change in oxidation state between the starting materials and the final cluster product. Considering Pd to begin in the 0 oxidation state and E to be trivalent, the final cluster stoichiometry requires the addition of 10 electrons. Elimination of Ph (either as Ph−H or Ph−Ph) could provide at least some of those electrons. Three possible overall stoichiometries are

$$4PdL_4 + 6Ph_2BiBr \rightarrow [Bi_4Pd_4L_8][Ph_2BiBr_2]_2 + 8L + 3Ph{-}Ph + 2Ph{-}Br$$

$$5PdL_4 + 6Ph_2BiBr \rightarrow [Bi_4Pd_4L_8][Ph_2BiBr_2]_2 + 10L + 4Ph{-}Ph + L_2PdBr_2$$

$$4PdL_4 + 7Ph_2BiBr \rightarrow [Bi_4Pd_4L_8][Ph_2BiBr_2]_2 + 8L + 5Ph{-}Ph + BiBr_3$$

Mass spectral results of the byproducts indicate the formation of Ph−Ph for E = Sb and Bi, and for E = Bi, a very small amount of PhX was also observed. This suggests that the first possibility does not represent the reaction stoichiometry, but given the low yield of the reaction and the instability of the product in solution, it is not possible to conclude more than this. When greater than a 1:1 ratio of Ph_2EX to PdL_4 was used in the starting reaction all that was isolated was L_2PdX_2.[76] Free phosphine was always found in the reaction solutions. Since an excess of Ph_2EX led to the formation of L_2PdX_2, it is not clear if that compound appears as a byproduct of the main reaction or results from subsequent reaction of the product cluster with Ph_2EX.

Electron Counting Considerations. The stable electron count for an E_4M_4 cubane is 80 electrons, which is the count predicted for conventional localized 2-center, 2-electron bonding. For the cases where bond formation occurs between transition metals, most of the compounds continue to obey the EAN formalism, i.e., M generally follows the 18-electron rule[77] and E obeys the octet rule consistent with Teo's analysis.[27] Each successive loss of two electrons is generally accompanied by the formation of one M−M bond, intermediate diamagnetic situations being sometimes observed.[30] Thus the TT_d $M_4(\mu_3\text{-}E)_4$ structure has 18 localized 2-electron, 2-center bonds (6 M−M + 12 M−E) and a resulting favored closed-shell cluster electron (CE) count of $(18 \times 4) + (8 \times 4) - (2 \times 18) = 68$. Conversely, starting with the 68-CE TT_d structure and breaking one M−M bond increases by two electrons the CE count until one arrives again at the 80-CE cubane structure.

The cluster core $[E_4(PdL_2)_4]^{2+}$ possesses a total of 74 electrons for which one would expect to obtain either one of the C_{3v} or C_2 structures (**5**, **6,** and **7**, respectively, in Scheme 1). The fact that it possesses a D_{2d} structure instead (**3** in Scheme 1) automatically indicates that a more delocalized bonding picture is required. Noting that **7** is closely related to the observed D_{2d} symmetry, one could analyze the compound as being a resonance hybrid of four structures of type **7** in which the missing E−E bond moves around the cluster framework. This would predict E−E bond orders of $^3/_4$, consistent with the long distances observed here compared to Sb−Sb and Bi−Bi single bonds.

In the TT_d $M_4(\mu_3\text{-}E)_4$ structure, localized 2-electron, 2-center bonding is possible because each transition metal atom has a set of nine valence orbitals, which is large enough to build six bonds within the cluster in addition to the metal−ligand bonds. This is not the case for the hypothetical TT_d $E_4(\mu_3\text{-}M)_4$ structure in which each main group atom has only four valence orbitals to ensure six cluster bonds and still retain a nonbonding lone pair. This is the typical situation for hypercoordination where

(72) Cisar, A.; Corbett, J. D. *Inorg. Chem.* **1977**, *16*, 2482.
(73) Zhuravlev, N. N. *Soviet Phys. JETP* **1957**, *5*, 1064.
(74) (a) Clegg, W.; Errington, J.; Fisher, G. A.; Hockless, D. C. R.; Norman, N. C.; Orpen, A. G.; Stratford, S. E. *J. Chem. Soc., Dalton Trans.* **1992**, 1967. (b) Clegg, W. R.; Errington, R. J.; Fisher, G. A.; Flynn, R. J.; Norman, N. C. *J. Chem. Soc., Dalton Trans.* **1993**, 637.
(75) Sheldrick, W. S.; Martin, C. *Z. Naturforsch* **1992**, *47b*, 919.
(76) Stark, J. L.; Whitmire, K. H. *Acta Crystallogr.* **1997**, *C53* (6), IUC9700007/1-2.
(77) Clusters with electron-deficient early-transition-metal centers have been reported. Their bonding is analyzed in ref 30.

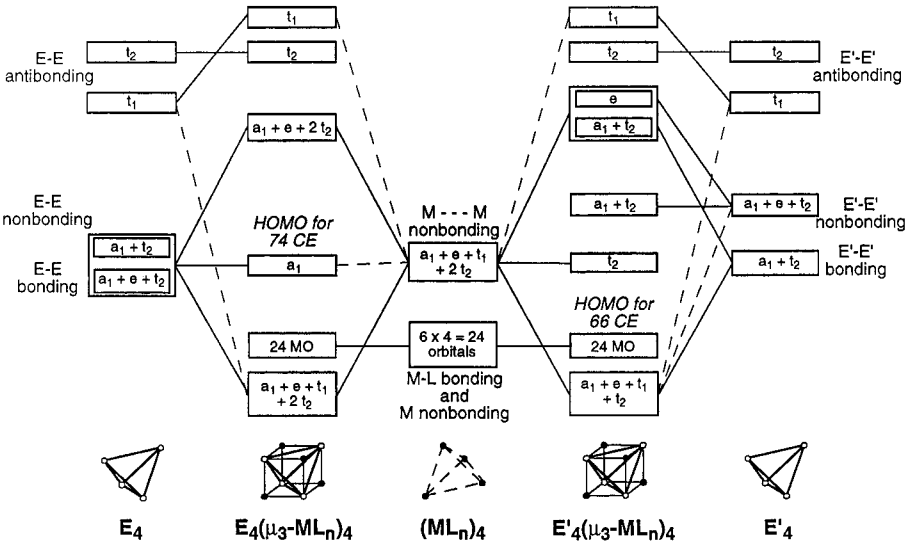

Figure 3. Qualitative MO interaction diagrams of a 74-CE $E_4(\mu_3\text{-}ML_n)_4$ cluster (left) and a 66-CE $E'_4(\mu_3\text{-}ML_n)_4$ cluster (right) (E′ = early main-group element).

each atomic orbital (or combination thereof) is participating in more than one bond or lone pair.[78] In such a situation the number of bonding MOs is lower than the number of bonding contacts. Therefore the CE count of the TT_d $M_4(\mu_3\text{-}E)_4$ structure is expected to be different from the one of its $E_4(\mu_3\text{-}M)_4$ homologue. Owing to the tendency of group 15 elements to show hypervalency, the CE count of the $E_4(\mu_3\text{-}M)_4$ (E = group 15 element) is expected to be larger than 68.

Qualitative Approach in Determining the Electronic Structure of a TT_d $E_4(\mu_3\text{-}M)_4$ Cluster. The electronic structure of an hypothetical $E_4(\mu_3\text{-}ML_n)_4$ cluster of T_d symmetry can be predicted as resulting from the interaction between two tetrahedra: an E_4 tetrahedron, in which the atoms are bonded, and an $(ML_n)_4$ tetrahedron made of four nonbonded metal atoms in their local environment of terminal ligands. In the first fragment, the four s and p AOs on each of the four E atoms combine to give rise to a set of six bonding combinations ($a_1 + e + t_2$), a set of four nonbonding combinations ($a_1 + t_2$), and a set of six antibonding levels ($t_1 + t_2$).[79,80] This well-known level ordering is drawn on the far left side of Figure 3. To cap symmetrically a triangular face of the E_4 tetrahedron, a transition metal atom needs three frontier orbitals, one of local σ-type and two of π-type symmetry.[80] This means that the six remaining metal AOs are involved in metal−terminal ligand bonding or hold the metal nonbonding lone pairs. Six electron pairs must then be associated with each ML_n group in addition to those lying in its three frontier orbitals. Because there is no interaction between the M atoms, these frontier orbitals give rise to 12 nonbonding combinations in the tetrahedral $(ML_n)_4$ fragment ($a_1 + e + t_1 + 2t_2$).[79] They correspond to the levels shown in the middle of Figure 3. To ensure strong M−E bonding, these metal levels must interact significantly with their E_4 counterparts. In a localized bonding scheme, they would interact only with the nonbonding levels of the E_4 fragment. Since in the present case there are only four ($a_1 + t_2$) E_4 nonbonding orbitals, eight other E_4 levels of e, t_1, and t_2 symmetries are also needed for the M−L interactions. They can be found in the bonding set ($e + t_2$) and in the antibonding t_1 set. The resulting skeletal MO interaction diagram expected for a hypothetical TT_d $E_4(\mu_3\text{-}ML_n)_4$ cluster is sketched in the left half of Figure 3. Only two E_4 levels are left nonbonding with respect to interaction with the metal fragments. One is one of the two E_4 a_1 orbitals (or a combination of these), the other one being the antibonding t_2 level, which one can anticipate to be too high in energy to interact significantly with the metal frontier orbitals. Closed-shell stability requires the filling of all the bonding and nonbonding levels, leaving the antibonding ones vacant. This corresponds to the occupation of the 13 lowest skeletal orbitals of the $E_4(\mu_3\text{-}ML_n)_4$ cluster. To these 26 electrons one has to add 12 electrons per metal center (vide infra), which leads to the favored 74-CE count for the TT_d $E_4(\mu_3\text{-}ML_n)_4$ cluster. This counts exceeds by six the corresponding value of the localized $M_4(\mu_3\text{-}E)_4$ TT_d species.

For this electron count, the interaction of the E−E bonding orbitals of the E_4 fragment with vacant counterparts on the $(ML_n)_4$ unit is expected to depopulate the former in the final cluster. On the other hand the vacant t_1 antibonding E−E orbitals of the E_4 fragment should be significantly populated after interaction through their participation in occupied skeletal cluster orbitals. Both effects are expected to weaken the E−E bonding as compared to E−E single bonds in an isolated 20-electron E_4 tetrahedron. This expected weakening is the result of hypercoordination.

Electronic Structure of the Hypothetical 74-CE TT_d $[Sb_4\{\mu_3\text{-}Fe(CO)_3\}_4]^{2+}$ Compound. To check the above qualitative analysis in a more quantitative way, we have performed extended Hückel theory (EHT) and density functional theory (DFT) calculations on the hypothetical 74-CE $[Sb_4\{\mu_3\text{-}Fe(CO)_3\}_4]^{2+}$ cluster, assuming first T_d molecular symmetry. Details of the calculations are given in the Experimental Section. The molecular geometry was fully optimized at the DFT level. It is shown in Figure 5a. The major optimized metrical data are reported in Table 4, together with the computed HOMO−LUMO gap. The EHT and DFT MO diagrams of $[Sb_4\{\mu_3\text{-}Fe(CO)_3\}_4]^{2+}$ are given on the left and right sides of Figure 4, respectively. The occupied levels that are shown are the Fe nonbonding and the highest Fe−Sb bonding combinations. The t_2 LUMO is the lowest skeletal Fe−Sb antibonding level. The other vacant levels shown have a dominant π^*(CO) character. It is noteworthy that both types of calculation are in close agreement, leading to similar electronic configurations, level

(78) Albright, T. A.; Burdett, J. K.; Whangbo, M.-H. *Orbital Interactions in Chemistry*; John Wiley and Sons: New York, 1985.

(79) Cotton, F. A. *Chemical Applications of Group Theory*, 3rd ed.; John Wiley and Sons: New York, 1990.

(80) Mingos, D. M. P.; Wales, D. J. *Introduction to Cluster Chemistry;* Prenctice Hall International Editions: Engelwood Cliffs, NJ, 1990.

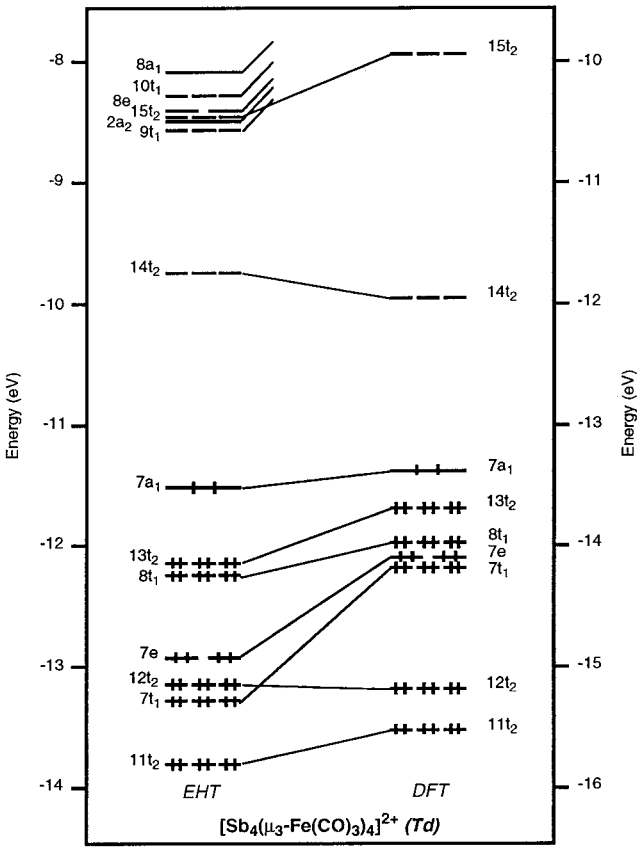

Figure 4. EHT and DFT MO level ordering of $[Sb_4\{\mu_3\text{-}Fe(CO)_3\}_4]^{2+}$.

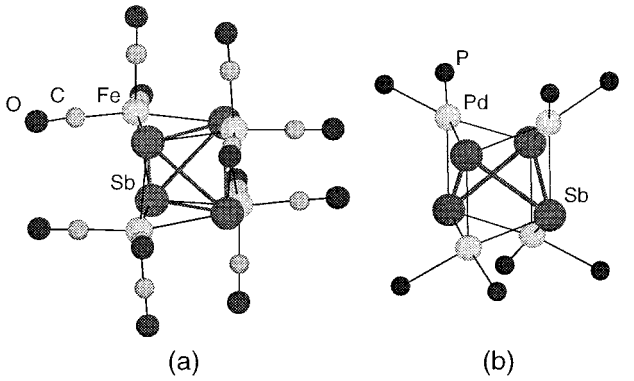

Figure 5. DFT-optimized molecular structures of (a) $[Sb_4Fe_4(CO)_{12}]^{2+}$ and (b) $[Sb_4Pd_4(PH_3)_8]^{2+}$.

ordering, and energy gaps. They are also in full agreement with the qualitative MO diagram of the $E_4(\mu_3\text{-}ML_n)_4$ cluster (left side of Figure 3). Both EHT- and DFT-computed HOMO−LUMO gaps are large, as expected from the qualitative predictions of the thermodynamical stability of 74-CE $E_4(\mu_3\text{-}ML_n)_4$ TT_d clusters and from earlier EHT calculations on the related $[Bi_4\{\mu_3\text{-}Fe(CO)_3\}_4]^{2+}$ model.[45] Nevertheless, the Jahn−Teller stability of the T_d architecture was tested by performing DFT geometry optimization assuming D_{2d} symmetry. The calculations provided the same T_d molecular geometry.

In agreement with its hypervalent coordination mode, the DFT-optimized Sb−Sb bond lengths (3.08 Å) are longer than what one would expect for a standard single bond**.** A significant bonding interaction is still present, however, as exemplified by the corresponding EHT overlap population (+0.253). The DFT-optimized Sb−Fe distances (2.61 Å) are in the range of those for normal single bonds. Clearly the calculations suggest

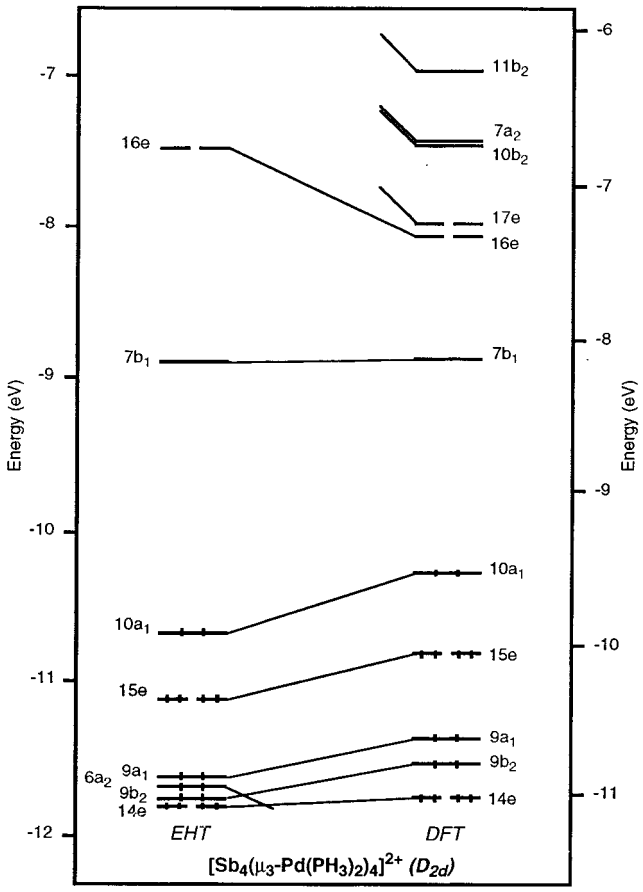

Figure 6. EHT and DFT MO level ordering of $[Sb_4\{\mu_3\text{-}Pd(PPH_3)_2\}_4]^{2+}$.

strongly that the hypothetical tetrahedral $[Sb_4\{\mu_3\text{-}Fe(CO)_3\}_4]^{2+}$ cluster may be synthesizable.

Electronic Structure of the 74-CE $[Sb_4(\mu_3\text{-}Pd(PH_3)_2)_4]^{2+}$ Model. EHT and DFT calculations have been carried out on $[Sb_4(\mu_3\text{-}Pd(PH_3)_2)_4]^{2+}$, as a model for compound **1**. Ideal D_{2d} symmetry was assumed. Details of the calculations are given in the Experimental Section. Important structural data obtained through the DFT geometry optimization are given in Table 4. The optimized structure is shown in Figure 5b. The optimized Pd−Sb distances are in a fairly good agreement with the experimental distances (Tables 2 and 4), the optimized Sb−Sb separations (3.15 and 3.54 Å) being slightly longer than the experimental ones. The EHT and DFT MO diagrams of $[Sb_4(\mu_3\text{-}Pd(PH_3)_2)_4]^{2+}$ are given in Figure 6 in a similar frontier region as for $[Sb_4\{\mu_3\text{-}Fe(CO)_3\}_4]^{2+}$ (see above). As for this latter model, both types of calculations give consistent results. In particular, both methods give large HOMO−LUMO gaps, in agreement with the stability of compounds **1** and **2**. The relative strength of the two types of Sb−Sb contacts can be evaluated by the corresponding computed EHT overlap populations which are 0.411 and 0.080 for the short (3.05 Å) and long (3.39 Å) separations, respectively. Clearly, the bonding along the two long edges of the Sb_4 tetrahedron is weak. The average value is close to the one computed for $[Sb_4\{\mu_3\text{-}Fe(CO)_3\}_4]^{2+}$. The EHT Pd−Sb overlap populations are 0.283 and 0.156 for the short (2.64 Å) and long (2.76 Å) separations, respectively. These values indicate that significant bonding is still present along the long Pd−Sb vectors.

One may wonder why the 74-CE clusters **1** and **2** adopt a D_{2d} geometry (**3** in Scheme 1), while theory predicts that an isoelectronic species such as $[Sb_4\{\mu_3\text{-}Fe(CO)_3\}_4]^{2+}$ should have

Table 4. Selected Structural Data and HOMO−LUMO Gaps Corresponding to the DFT-Optimized Geometries of Various Closed-Shell $E_4(ML_n)_4$ Model Clusters

	$[Sb_4Pd_4(PH_3)_8]^{2+}$ 74 CE, D_{2d}	$[Sb_4Fe_4(CO)_{12}]^{2+}$ 74 CE, T_d	$Sb_4Co_4(CO)_{12}$ 80 CE, T_d	$Bi_4Co_4(CO)_{12}$ 80 CE, T_d	$[Ga_4Fe_4(CO)_{12}]^{2+}$ 66 CE, T_d	$[In_4Fe_4(CO)_{12}]^{2+}$ 66 CE, T_d	$[Tl_4Fe_4(CO)_{12}]^{2+}$ 66 CE, T_d
M−E (Å)	2.69−2.82	2.61	2.64	2.74	2.43	2.59	2.69
E−E (Å)	3.15−3.54	3.08	3.23	3.42	3.33	3.56	3.70
M−E−M (deg)	84.6−110.3	105.1	102.9	101.3	93.4	93.1	93.2
E−M−E (deg)	69.7−82.3	72.4	75.3	77.4	86.5	86.8	86.7
M−L (Å)	2.37	1.78	1.78	1.78	1.81	1.79	1.80
P−H/C−O (Å)	1.43	1.14	1.15	1.15	1.14	1.15	1.15
L−M−L (deg)	93.7	95.3	102.9	103.1	99.6	102.2	103.3
HOMO/LUMO gap (eV)	1.34	1.42	2.10	2.23	0.88	0.89	0.84

the TT_d structure (**1** in Scheme 1). Examination of the skeletal orbitals of $[Sb_4\{\mu_3\text{-}Pd(PH_3)_2\}_4]^{2+}$ indicates that it has the same electron configuration than $[Sb_4\{\mu_3\text{-}Fe(CO)_3\}_4]^{2+}$, i.e. when going from the latter TT_d cluster to the former D_{2d} compound there is no HOMO−LUMO level crossing. The T_d to D_{2d} lowering in symmetry perturbs somewhat the level ordering within the occupied MOs as well as within the vacant MOs, but maintains a large gap between these two blocks. The reason for the significant D_{2d} distortion of the E_4 tetrahedron present in the core of **1** and **2** originates from the nonconical nature of the PdL_2 fragments.[77] As said above, the capping of a triangular face of an E_4 tetrahedron by a metal fragment requires, inter alia, the use of two metal π-type frontier orbitals. A symmetrical capping requires degeneracy of these two orbitals. In the case of the PdL_2 fragment, one is far from this situation. One of its π frontier orbitals is a low-lying d-type hybrid, which lies in the PdL_2 plane and whose main lobes are pointing in the direction of the long Sb···Sb edges. The other π frontier orbital is the high-lying Pd $5p_z$ orbital which is perpendicular to the PdL_2 plane. Because of a better energy match and of better directional properties, the d-type orbital interacts more strongly with the triangular face than the p-type orbital. As a result, an unsymmetrical capping and a distortion of the E_4 tetrahedron occur. The two Sb−Sb edges which are in a privileged position to interact with the four d-type metal orbitals are much more perturbed. As a result, the Sb−Sb σ-donation and σ*-retrodonation (see qualitative approach) affect preferencially these two Sb−Sb edges. The effect is strong enough to almost cancel the corresponding Sb−Sb bonding. On the other hand, the four other edges which are involved with the weaker interaction with the metal p-type orbital, are less perturbed. Thus, clusters **1** and **2** are better described as strongly distorted relatives of the TT_d structure **1** of Scheme 1, rather than typical representatives of a new structural type of D_{2d} symmetry (**3** in Scheme 1).

Another Possible Closed-Shell CE Count for the TT_d $E_4(\mu_3\text{-}M)_4$ Geometry. In a search for alternative stable electron counts for a $E_4(\mu_3\text{-}M)_4$ cluster having structure **1** of Scheme 1, EHT calculations on a series of $E_4(\mu_3\text{-}M(CO)_3)_4$ models, with M varying from V to Ni and E varying from group 13 to group 15 have been carried out. These exploratory calculations suggested that another CE count, namely 66, should be favored for this TT_d arrangement. This situation is expected to occur with early main-group elements. The qualitative MO interaction diagram of such a $E'_4(\mu_3\text{-}ML_n)_4$ species is sketched in the right half of Figure 3. In the case of an early main-group E'_4 tetrahedron, the mixing between the s-type combinations and the high-lying p-type combinations is weak. As a result, the 10 lowest orbitals of E'_4 are split into two groups, well-separated in energy. The lowest set is significantly bonding and can be described as made of the $a_1 + t_2$ combinations of the s atomic orbitals. Although weakly bonding or nonbonding, the other set ($a_1 + e + t_2$) lies at a rather high energy since it derives primarily from the high-lying p atomic orbitals. This level ordering is depicted on the right side of Figure 3. The EHT calculations indicate that the $a_1 + e + t_1 + 2t_2$ set of frontier orbitals of the tetrahedral $(ML_n)_4$ fragment matches with the lowest $a_1 + t_2$ E'_4 orbitals and with the unique e and t_1 sets of the E'_4 fragment. The E'_4 high-lying t_2 level is only weakly involved in the interaction. As a consequence, one of the t_2 sets of the $(ML_n)_4$ fragment remains nonbonding. The resulting MO level ordering exhibits a group of nine M−E′ bonding orbitals ($a_1 + e + t_1 + t_2$) well-separated from the nonbonding t_2 level. A large HOMO−LUMO gap is found when the bonding block is filled and the nonbonding t_2 set remains vacant. This 66-CE situation corresponds to an electron-deficient system since there are only nine bonding electron pairs associated with 12 M−E′ bonding contacts. DFT calculations on the hypothetical TT_d $[E'_4(\mu_3\text{-}Fe(CO)_3)_4]^{2+}$ (E′ = Ga, In, Tl) series confirm the EHT expectations. The computed HOMO−LUMO gaps and major optimized metrical data are reported in Table 4. In the case of E′ = In and Tl, the optimized E′−E′ distances are slightly longer than in the metal (3.56 and 3.70 Å vs 3.25 and 3.40 Å, respectively). In the case of E′ = Ga, the corresponding value is significantly larger that in the metal (3.33 vs 2.45 Å). In the three compounds, the M−E′ distances are in the range of expected values for regular bonds. Significant HOMO−LUMO gaps are computed, indicating closed-shell stability. These results strongly suggest that 66-CE TT_d $E_4(\mu_3\text{-}M)_4$ clusters should be accessible.

Adding Electrons to the 74-CE TT_d $E_4(\mu_3\text{-}M)_4$ Arrangement. As said above, in the case of the various structures of Scheme 1 deriving from the $M_4(\mu_3\text{-}E)_4$ TT_d geometry, one goes from the favored closed-shell count of 68 CE (**1**) to 80 CE (**11**) by adding two electrons to the CE count as one sucessively breaks the M−M bonds. In the case of the possible structures deriving from the $E_4(\mu_3\text{-}M)_4$ TT_d geometry, the largest electron count still corresponds to the 80-CE cubane species. One may ask if, between the CE counts of 74 (**1**) and 80 (**11**), other stable intermediate arrangements (such as **2**−**10** in Scheme 1) could exist for particular closed-shell CE counts. Exploratory EHT calculations on various $E_4M_4(CO)_{12}$ models were not able to reproduce particular compounds with structures **2**−**10** for which the existence of a large HOMO−LUMO gap would clearly indicate fulfillment of the closed-shell requirement. Some DFT calculations performed on 76- and 78-CE systems confirmed the EHT results. Stable closed-shell situations were only found for the known 80-CE cubane-type structure **11**. The major structural data of the DFT optimized structures and the corresponding HOMO−LUMO gaps of the 80-CE cubane-type compounds $[Co_4(CO)_{12}(\mu_3\text{-}E)_4]$ (E = Bi, Sb) are given in Table 4. The optimized geometries are in good agreement with the experimental ones.[16,17] These results support the suitability of using DFT calculations for predicting molecular structures in this class of compounds and suggest that stable closed-shell

E_4M_4 clusters presenting E−E bonding with structures **2**−**10** are unlikely to exist for CE counts intermediate between 74 and 80. This does not rule out, however, the possibility of existence of paramagnetic species.

Conclusions. The 74-CE clusters $[E_4(PdL_2)_4]^{2+}$ (E = Sb, Bi) have a core arrangement corresponding to structure **3** of Scheme 1 and deriving from the $E_4(\mu_3\text{-}M)_4$ TT_d structure **1** by the almost complete breaking of two E−E bonds. Calculations on the model $[Sb_4(Pd(PH_3)_2)_4]^{2+}$ indicate that these compounds are electronically strongly related to the isoelectronic hypothetical $[Sb_4(\mu_3\text{-}Fe(CO)_3)_4]^{2+}$ TT_d species. The lower D_{2d} symmetry of the $[E_4(PdL_2)_4]^{2+}$ (E = Sb, Bi) systems is the consequence of the nonconical nature of the PdL_2 constituents of the clusters. In particular, the existence in these clusters of two long E···E separations is principally due to the strong d-π donation of the PdL_2 units into the σ*(E···E) orbitals. 74-CE TT_d $E_4(\mu_3\text{-}ML_n)_4$ clusters are predicted to be stable diamagnetic compounds in which the presence of both E−E and M−E bonding is the consequence of the tendency to hypervalency of heavy main-group elements. The $E_4(\mu_3\text{-}M)_4$ TT_d arrangement (structure **1** in Scheme 1) should also be stable for the closed-shell 66-CE count. Such an electron-poor system is favored with early main-group elements. The formal adding of electrons to a 74-CE $E_4(\mu_3\text{-}ML_n)_4$ TT_d species is expected to induce E−E bond breaking and successively generates structures **2**−**11** (Scheme 1). Calculations indicate that there is no CE count intermediate between 74 and 80 which fulfills the closed-shell requirement for structures **2**−**10**, assuming conical ML_n units.

Acknowledgment. The Centre National de la Recherche Scientifique (J.-Y.S. and J.-F.H.) and the National Science Foundation (K.H.W.) are gratefully acknowledged for financial support of this work as well as for the cooperative international travel grant that has greatly facilitated these studies. The Robert A. Welch Foundation (K.H.W.) also provided financial support for carrying out these studies. J.-F.H. and J.-Y.S. thank Pr. Baerends and Dr. te Velde (Vrije Universiteit, Amsterdam) for introducing them to the ADF program. Exchanges with Baerends' group have been made possible through a European Human Capital and Mobility Network Grant. J.-F.H. and J.-Y.S. thank the Centre de Ressources Informatiques of Rennes and the Institut de Developpement et de Ressources en Informatique Scientifique of Orsay for computing facilities.

Supporting Information Available: Tables of crystal data and structural refinements, anisotropic and isotropic thermal parameters, full bond distances and angles, and atomic coordinates, labeling scheme diagrams, and full thermal ellipsoid plots for the cations and anions of $[Sb_4(PdL_2)_4][Ph_2SbCl_2]_2 \cdot 0.5THF$ and $[Bi_4(PdL_2)_4][Ph_2BiBr_2]_2$ (PDF). This material is available free of charge via the Internet at http://pubs.acs.org.

JA982902U